C. R. Mecanique 346 (2018) 1216–1232

Contents lists available at ScienceDirect

Comptes Rendus Mecanique

www.sciencedirect.com

Damped vibration of a graphene sheet using a higher-order nonlocal strain-gradient Kirchhoff plate model

Davood Shahsavari [a], Behrouz Karami [a,*], Li Li [b,*]

[a] Department of Mechanical Engineering, Marvdasht Branch, Islamic Azad University, Marvdasht, Iran
[b] State Key Lab of Digital Manufacturing Equipment and Technology, School of Mechanical Science and Engineering, Huazhong University of Science and Technology, Wuhan 430074, China

ARTICLE INFO

Article history:
Received 22 May 2018
Accepted 24 August 2018
Available online 5 September 2018

Keywords:
Damped vibration
Bi-Helmholtz nonlocal strain gradient theory
Environmental effects
Graphene
Visco-Pasternak foundation

ABSTRACT

A higher-order nonlocal strain-gradient model is presented for the damped vibration analysis of single-layer graphene sheets (SLGSs) in hygrothermal environment. Based on Kirchhoff plate theory in conjunction with a higher-order (bi-Helmholtz) nonlocal strain gradient theory, the equations of motion are obtained using Hamilton's principle. The higher-order nonlocal strain gradient theory has lower- and higher-order nonlocal parameters and a material characteristic parameter. The presented model can reasonably interpret the softening effects of the SLGS, and indicates a reasonably good match with the experimental flexural frequencies. Finally, the roles of viscous and structural damping coefficients, small-scale parameters, hygrothermal environment and elastic foundation on the vibrational responses of SLGSs are studied in detail.

1. Introduction

Graphene sheets (GSs) have drawn considerable attention due to numerous advantages for their use in sensitive devices such as nanoelectromechanical systems (NEMS) [1], biological tissue [2], nanosensors [3], and nanoactuators [4]. The single-layer graphene sheet (SLGS) is one of the popular graphene-based materials and is known as a two-dimensional flat monolayer with nanoscale. When the scale of a structure such as a plate reduces to the nanometer scale, the size-dependent effects play an important role on the mechanical behavior of the structure (see some of points in Refs. [5,6]).

Over the last few years, different non-classical continuum theories have been introduced to examine size-dependent effects [7–11]. Amongst them, nonlocal elasticity theory [12], as a popular model of non-classical continuum theories, can account for long-range interatomic forces. On the basis of the nonlocal elasticity theory, a great deal of researches have been focused on analyzing the size-dependent mechanical and physical behaviors of various nanoscale structures, including nanobeam, nanoplate, and nanoshell [13–27]. Recently, in the endless development of these theories, bi-Helmholtz nonlocal continuum theory [28], which has two distinct nonlocal parameters (so-called low- and high-order nonlocal parameters) has been used to analyze the dynamical response of carbon nanotubes [29]. These authors concluded that the bi-Helmholtz nonlocal model is more appropriate than the one-parameter nonlocal model (nonlocal elasticity theory) for measuring the softening effects in carbon nanotubes by using molecular dynamics (MD) simulation results. Moreover, Shaat and Abdelkefi [30] showed that nonlocal continuum theory with one nonlocal parameter cannot show a good match with both longitu-

* Corresponding authors.
E-mail addresses: Shahsavari.davood@miau.ac.ir (D. Shahsavari), behrouz.karami@miau.ac.ir (B. Karami), lili_em@hust.edu.cn (L. Li).

https://doi.org/10.1016/j.crme.2018.08.011
1631-0721/

dinal and flexural wave dispersions of experimental data, and the bi-Helmholtz nonlocal model was suggested for a better accuracy. Also, Barretta et al. [31] used two pairs of nonlocal parameters (lower and higher order) to model the functionally graded nanobeam.

In spite of the mentioned advantages about nonlocal continuum models, the capacity of these nonlocal models to satisfy other size-dependent effects on the mechanical properties of nanostructures has some limitations [32]. For instance, by applying nonlocal continuum theory, the stiffness-enhancement effect, which was observed from strain gradient elasticity theory [5] and experimental data [33], cannot be predicted well. In fact, the strain gradient elasticity theory states that the strain in a point is a function of all stresses in its neighbor points [34]. According to this theory, the role of size effect is also measured with only one small-scale parameter (known as material characteristic parameter). Mathematically, on the basis of Hooke's law, the nonlocal parameter is located in the Laplacian of stress on the left-hand side of the fundamental equation, whereas the material characteristic parameter is used on the right-hand side of the fundamental equation on the Laplacian of strains [35].

A nonlocal strain gradient theory is proposed by Aifantis [36] to examine both the stress gradient effect and the strain gradient effect in small-scale structures. This theory can estimate both the softening-stiffness and stiffness-enhancement effects. Challamel and Wang [37] used the nonlocal strain gradient theory to overcome the paradox in nonlocal cantilever beams subjected to a point load. Zhang et al. [38] examined the bending, buckling, and vibration of nonlocal strain gradient beams. Jafari et al. [39] studied the vibration behavior of nonlocal strain gradient plates. In the context of thermodynamics framework, Lim et al. [32] cast both the stress-gradient and strain-gradient effects into a higher-order (bi-Helmholtz) nonlocal strain gradient theory. The bi-Helmholtz nonlocal strain gradient beam model [32] showed good agreement between the theoretical results and the MD results for carbon nanotubes. Recently, Ebrahimi et al. [40] studied the vibration behavior of nonlocal strain-gradient plates made of functionally graded material. Up to now, many scholars have been trying to use this model for studying the mechanical behavior of elastic nanoparticles [41], nanorod [42], nanoshells [43], nanobeams [32,44,45] and nanoplates [46,47] under the influence of thermal environment [40], hygrothermal environment [48,49], magnetic field [50,51], elastic substrate [40], and viscoelastic substrate [18]. The bi-Helmholtz nonlocal strain gradient theory containing three distinct small-scale parameters has been employed to examine the wave propagation in porous double-nanobeam systems in the presence [52] and absence [53] of thermal environments. Farajpour et al. [54] examined higher-order nonlocal strain gradient theory for the buckling analysis of nanoplates. This size-dependent model based on a quasi-3D plate theory was used for the wave propagation analysis of nanoplates made of functionally graded material [55]. Most recently, the effectiveness of this theory in the wave frequency of SLGS was examined by Karami et al. [35] by comparing results between numerical and experimental data.

In practical, structures often work under the influence of environmental conditions. The concept of environmental conditions can cover wet-dry, freeze-thaw, sea-water, and moisture impression. Among them, the temperature and absorption of moisture are most important conditions for the accurate analysis of GSs. Many studies were conducted to develop mechanical models of GSs incorporating the influence of environmental conditions. For instance, the elastic material properties of zigzag and armchair GSs involving the influence of temperature have been estimated using MD simulation by Shen et al. [15], which showed that the material properties of SLGSs are temperature-dependent and size-dependent. With the estimated elastic material properties, the static deflections [56] and frequency [15] of GSs were determined under temperature effect by MD simulation as well as nonlocal elasticity models. They showed that the nonlocal elasticity theory can be used to predict the mechanical behavior of SLGSs in the thermal environment when an appropriate nonlocal parameter is chosen. Since other environmental conditions are important on the response of SLGSs, Han et al. [57] investigated the moisture-response of SLGSs by performing self-controlled photoreduction experimentally. This study showed that the SLGS exhibits moisture-responsive properties owing to the selective adsorption of water molecules. Additionally, the effects of environment attacks due to elevated temperature and absorbed moisture on the nonlocal static [58], dynamic [18], vibration [59], wave propagation [35,49], and buckling [48] analysis of SLGSs have been conducted analytically. It was reported that the nonlocal effect plays a very important role on the mechanical behaviors of SLGS in the temperature and moisture environment.

A foundation can be used as a controller for these structures under an environmental condition. Up to now, various hypotheses of elastic foundations for describing the interaction between foundation and plate have been used (see some of them in Ref. [60]). The simplest model of elastic foundation has just one coefficient medium reaction (known as Winkler elastic foundation). This model is imperfect in providing continuity in the medium due to separate springs [61]. To overcome the previously mentioned imperfection, Pasternak's model was presented by adding a shear layer over springs. In addition, when considering a viscous damping constant, a portion of energy can be irrecoverable [62]. Therefore, the construction including viscoelastic foundation is more effective, especially on creep behavior [63]. Hence, a great deal of researches have been carried out for modeling nanostructures, resting on visco-Pasternak foundation [18,35,59,64].

Up to now, no analytical study in the open literature has been tried to propose a bi-Helmholtz nonlocal strain-gradient model for the hygro-thermo-viscoelastic vibration of nanoplates. Hence, this study will present a bi-Helmholtz nonlocal strain-gradient model to examine the influences of heat as well as of the moisture conduction field on the complex frequency of a viscoelastic orthotropic nanoplate surrounded by a visco-Pasternak foundation. The developed model shows a reasonably good match with the experimental flexural frequencies, and hence can reasonably interpret the softening effects of the flexural frequencies of the SLGS. Finally, the roles of viscous and structural damping coefficients, small-scale

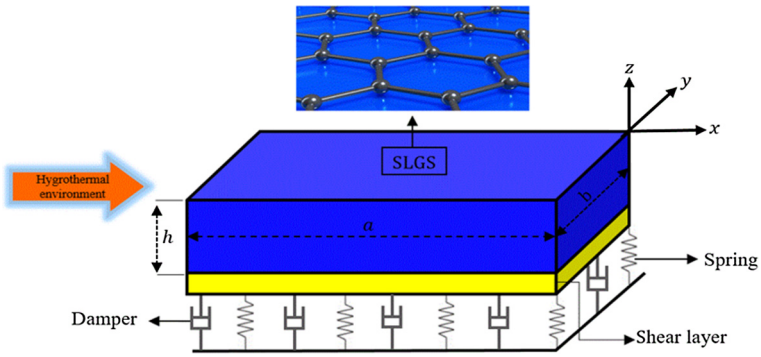

Fig. 1. A viscoelastic SLGS coupled with a visco-Pasternak foundation within a hygrothermal environment.

parameters, hygrothermal environment, and elastic foundation on the vibrational frequencies of SLGSs will be investigated in detail.

2. Problem definition and fundamental equations

Consider a simply supported nanoplate with viscoelastic orthotropic material and geometry, which is shown in Fig. 1. As shown in Fig. 1, the nanoplate is referred to the (x, y, z) set of directions, where the z-axis is along the thickness. Moreover, it is exposed to the hygrothermal environment and rests on a visco-Pasternak foundation.

2.1. Bi-Helmholtz nonlocal strain gradient theory

Based on the popular model of nonlocal strain gradient elasticity theory [36], the stress of elastic materials depends on the nonlocal elastic stress field as well as the strain gradient stress field

$$t = \sigma - \nabla\sigma^{(1)} \tag{1}$$

in which the nonlocal elastic stress field σ corresponds to the strain tensor ε; and the higher-order stress tensor $\sigma^{(1)}$ corresponds to the strain gradient sensor $\nabla\varepsilon$. That is,

$$\begin{aligned}\sigma &= \int_V \alpha_0(x', x, e_0 a) C : \varepsilon' \mathrm{d}V' \\ \sigma^{(1)} &= l^2 \int_V \alpha_1(x', x, e_1 a) C : \nabla\varepsilon' \mathrm{d}V'\end{aligned} \tag{2}$$

where ':' is the double-dot product, l denotes a material characteristic parameter (in some available literature, it is also known as the length-scale parameter or gradient parameter [65]) that allows us to consider the magnitude of the higher-order strain gradient stress field. Moreover, $e_0 a$ and $e_1 a$ are the low- and high-order nonlocal parameters that are reported from atomic lattice dynamics or experimental data by matching the wave dispersion relation to consider the magnitude of the nonlocal elastic stress field. Also, $\alpha_0(x, x', e_0 a)$ and $\alpha_1(x, x', e_1 a)$ are the nonlocal kernel functions.

With some simplification, the constitutive relation of nonlocal strain gradient theory has the following form [40]:

$$\left[1 - (e_1 a)^2 \nabla^2\right]\left[1 - (e_0 a)^2 \nabla^2\right] t_{ij} = Q_{ijkl}\left[1 - (e_1 a)^2 \nabla^2\right]\varepsilon_{kl} - Q_{ijkl}\kappa^2\left[1 - (e_0 a)^2 \nabla^2\right]\nabla^2\varepsilon_{kl} \tag{3}$$

Let $\mu_0 = e_0 a$ and $\mu_1 = e_1 a$, bi-Helmholtz nonlocal strain gradient elasticity theory can be formulated as [32]:

$$\left(1 - \mu_1^2\nabla^2\right)\left(1 - \mu_0^2\nabla^2\right) t_{ij} = Q_{ijkl}\left[\left(1 - \mu_1^2\nabla^2\right)\varepsilon_{kl} - l^2\left(1 - \mu_0^2\nabla^2\right)\nabla^2\varepsilon_{kl}\right] \tag{4}$$

To examine the role of heat and moisture on the vibrational response of orthotropic nanoplates, the hygrothermal effect is added to the constitutive relation as follows [35]

$$\left(1 - \mu_1^2\nabla^2\right)\left(1 - \mu_0^2\nabla^2\right) t_{ij} = Q_{ijkl}\left[\left(1 - \mu_1^2\nabla^2\right)\varepsilon_{kl} - \alpha_{ij}\Delta T - \beta_{ij}\Delta H - l^2\left(1 - \mu_0^2\nabla^2\right)\nabla^2\varepsilon_{kl}\right] \tag{5}$$

here $\Delta T = T - T_0$ and $\Delta H = H - H_0$ signify the thermal and moisture rises, respectively. (T_0, H_0) denote the reference temperature and moisture concentration, respectively. (T, H) denote the final temperature and moisture concentration, respectively. It can be of interest that the simpler models of Eq. (5) based on nonlocal elasticity theory or strain gradient elasticity theory be rendered by setting $\mu_0 = \mu_1 = 0$ and $l = 0$ in Eq. (5), respectively.

2.2. Hygrothermal environment

Hygrothermal environment effects on the formulation can be taken into account by introducing axial forces f_{ij}, which can be given as follows [15]:

$$\begin{aligned}
&f_{xx} = N_{xx}^{\mathrm{H}} + N_{xx}^{\mathrm{T}}, \qquad N_{xx}^{\mathrm{H}} = \int_{-\frac{h}{2}}^{\frac{h}{2}} \beta_{xx}\Delta H \mathrm{d}z, \qquad N_{xx}^{\mathrm{T}} = \int_{-\frac{h}{2}}^{\frac{h}{2}} \alpha_{xx}\Delta T \mathrm{d}z \\
&f_{yy} = N_{yy}^{\mathrm{H}} + N_{yy}^{\mathrm{T}}, \qquad N_{yy}^{\mathrm{H}} = \int_{-\frac{h}{2}}^{\frac{h}{2}} \beta_{yy}\Delta H \mathrm{d}z, \qquad N_{yy}^{\mathrm{T}} = \int_{-\frac{h}{2}}^{\frac{h}{2}} \alpha_{yy}\Delta T \mathrm{d}z \\
&f_{xy} = N_{xy}^{\mathrm{H}} + N_{xy}^{\mathrm{T}}, \qquad N_{xy}^{\mathrm{H}} = \int_{-\frac{h}{2}}^{\frac{h}{2}} \beta_{xy}\Delta H \mathrm{d}z, \qquad N_{xy}^{T} = \int_{-\frac{h}{2}}^{\frac{h}{2}} \alpha_{xy}\Delta T \mathrm{d}z
\end{aligned} \tag{6}$$

where (N_{xx}^{H}, N_{yy}^{H}, and N_{xy}^{H}) are the humidity efficacies due to absorbed moisture [15], and (N_{xx}^{T}, N_{yy}^{T}, and N_{xy}^{T}) are the thermal efficacies due to temperature change along the thickness of plate [66]. α_{xx}, α_{yy}, α_{xy}, β_{xx}, β_{yy} and β_{xy} indicate the thermal and moisture expansion coefficients in the x–x, y–y, and x–y surfaces, respectively. The thermal and moisture expansion coefficients can be specified as follows [15]:

$$\begin{bmatrix} \alpha_x & \beta_x \\ \alpha_y & \beta_y \\ \alpha_{xy} & \beta_{xy} \end{bmatrix} = - \begin{bmatrix} \bar{Q}_{11} & \bar{Q}_{12} & \bar{Q}_{16} \\ \bar{Q}_{12} & \bar{Q}_{22} & \bar{Q}_{26} \\ \bar{Q}_{16} & \bar{Q}_{26} & \bar{Q}_{66} \end{bmatrix} \begin{bmatrix} c^2 & s^2 \\ s^2 & c^2 \\ 2cs & -2cs \end{bmatrix} \begin{bmatrix} \alpha_{11} & \beta_{11} \\ \alpha_{22} & \beta_{22} \end{bmatrix} \tag{7}$$

here α_{11}, α_{22}, β_{11}, and β_{22} are the coefficients of thermal and moisture expansions in the longitudinal and transverse directions. Moreover, in the previous equation, the transformed elastic constants $\bar{Q}_{ij}$ corresponding to orthotropic materials are defined as [15]:

$$\begin{bmatrix} \bar{Q}_{11} \\ \bar{Q}_{12} \\ \bar{Q}_{22} \\ \bar{Q}_{16} \\ \bar{Q}_{26} \\ \bar{Q}_{66} \end{bmatrix} = \begin{bmatrix} c^4 & 2c^2s^2 & s^4 & 4c^2s^2 \\ c^2s^2 & c^4+s^4 & c^2s^2 & -4c^2s^2 \\ s^4 & 2c^2s^2 & c^4 & 4c^2s^2 \\ c^3s & cs^3-c^3s & -cs^3 & -2cs(c^2-s^2) \\ cs^3 & c^3s-cs^3 & -c^3s & 2cs(c^2-s^2) \\ c^2s^2 & -2c^2s^2 & c^2s^2 & (c^2-s^2)^2 \end{bmatrix} \begin{bmatrix} Q_{11} \\ Q_{12} \\ Q_{22} \\ Q_{66} \end{bmatrix} \tag{8}$$

in which the elastic constants Q_{ij} of orthotropic nanoplates can be specified by [62]:

$$Q_{11} = \frac{E_1}{(1-\nu_{12}\nu_{21})}, \qquad Q_{22} = \frac{E_2}{(1-\nu_{12}\nu_{21})}, \qquad Q_{12} = \frac{E_1\nu_{12}}{(1-\nu_{12}\nu_{21})}, \qquad Q_{66} = G_{12} \tag{9}$$

where $c = \cos(\theta)$, $s = \sin(\theta)$; and θ indicates the skew angle with respect to the x-axis of the plate.

3. Governing equations for rectangular nanoplates

3.1. Displacement field and strains

Based on Kirchhoff plate theory [67], the displacements of an arbitrary point of the structure can be defined in terms of the middle-surface displacement components. Therefore, the displacement field can be specified by

$$\begin{aligned}
u(x,y,z,t) &= u_0(x,y,t) - z\frac{\partial w_0}{\partial x} \\
v(x,y,z,t) &= v_0(x,y,t) - z\frac{\partial w_0}{\partial y} \\
w(x,y,z,t) &= w_0(x,y,t)
\end{aligned} \tag{10}$$

here the time-dependent variables u, v, and w are the middle surface displacement components in the x, y, and z directions, respectively.

According to the above displacement field, the strain–displacement relations in the nanoplate are expressed as

$$\begin{aligned}\varepsilon_{xx} &= \varepsilon^0_{xx} + \varepsilon^1_{xx}\\ \varepsilon_{yy} &= \varepsilon^0_{yy} + \varepsilon^1_{yy}\\ \gamma_{xy} &= \gamma^0_{xy} + z\gamma^1_{xy}\end{aligned} \tag{11}$$

here,

$$\begin{aligned}&\varepsilon^0_{xx} = \frac{\partial u}{\partial x}, \qquad \varepsilon^0_{yy} = \frac{\partial v}{\partial y}, \qquad \gamma^0_{xy} = \frac{\partial u}{\partial y} + \frac{\partial v}{x}\\ &\varepsilon^1_{xx} = -\frac{\partial^2 w}{\partial x^2}, \qquad \varepsilon^1_{yy} = -\frac{\partial^2 w}{\partial y^2}, \qquad \gamma^1_{xy} = -2\frac{\partial^2 w}{\partial x \partial y}\end{aligned} \tag{12}$$

in which ε_{xx} and ε_{yy} denote the normal strain members in the x and y directions, respectively, and ε_{xy} shows the shear strain part in the x–y plane. The classical stress–strain relation for an orthotropic elastic nanoplate under hygrothermal effect can be obtained as

$$\begin{bmatrix}\sigma_{xx}\\ \sigma_{yy}\\ \tau_{xy}\end{bmatrix} = \begin{bmatrix}\frac{E_1}{(1-\nu_{12}\nu_{21})} & \frac{\nu_{12}E_2}{(1-\nu_{12}\nu_{21})} & 0\\ \frac{\nu_{12}E_2}{(1-\nu_{12}\nu_{21})} & \frac{E_2}{(1-\nu_{12}\nu_{21})} & 0\\ 0 & 0 & G_{12}\end{bmatrix}\begin{bmatrix}\varepsilon_{xx}\\ \varepsilon_{yy}\\ \gamma_{xy}\end{bmatrix} - \begin{bmatrix}\alpha_x\Delta T + \beta_x\Delta H\\ \alpha_y\Delta T + \beta_y\Delta H\\ \alpha_{xy}\Delta T + \beta_{xy}\Delta H\end{bmatrix} \tag{13}$$

where σ_{xx}, σ_{yy}, and τ_{xy} are the normal and shear stresses in the x–y plane. E_1, E_2 are mean Young's modulus in the x and y directions, respectively, ν_{12}, ν_{21} indicate Poisson's ratios, and G_{12} denotes the shear modulus in the x–y surface.

The Voigt model assumes a uniform distribution of the displacement strain. Hence, the elastic moduli E_i and the shear modulus G_{ij} of viscoelastic materials relying on the Kelvin–Voigt model [68] can be redefined as [62]

$$E_i \leftarrow E_i\left(1 + g\frac{\partial}{\partial t}\right) \quad (i = 1, 2), \qquad G_{ij} \leftarrow G_{ij}\left(1 + g\frac{\partial}{\partial t}\right) \quad (i \neq j = 1, 2) \tag{14}$$

where g is the structural damping coefficient.

3.2. Equation of motion

The Hamilton energy principle given below will be applied for deriving the equation of motion of the nanoplate,

$$\int_{t_1}^{t_2} (\delta U + \delta W - \delta K)\mathrm{d}t = 0 \tag{15}$$

in which K, W, and U are kinetic energy, external work caused by the external force, and strain energy, respectively. In the following, these terms will be given in detail.

Taking the first variation of the evaluated strain energy leads to:

$$\begin{aligned}\delta U &= \int_V \left(\sigma_{xx}\delta\varepsilon_{xx} + \sigma_{yy}\delta\varepsilon_{yy} + 2\sigma_{xy}\delta\varepsilon_{xy} + \sigma^{(1)}_{xx}\nabla\delta\varepsilon_{xx} + \sigma_{yy}\delta\varepsilon_{yy} + \sigma_{yy}\delta\varepsilon_{xy}\right)\mathrm{d}V\\ &= \int_V \left(\left(\sigma_{xx} - \nabla\sigma^{(1)}_{xx}\right)\delta\varepsilon_{xx} + 2\left(\sigma_{xy} - \nabla\sigma^{(1)}_{xy}\right)\delta\varepsilon_{xy} + \left(\sigma_{yy} - \nabla\sigma^{(1)}_{yy}\right)\delta\varepsilon_{yy}\right)\mathrm{d}V\\ &\quad + \left[\int_0^b \left(\int_{-h/2}^{h/2} \sigma^{(1)}_{xx}\nabla\delta\varepsilon_{xx}\mathrm{d}z + 2\int_{-h/2}^{h/2} \sigma^{(1)}_{xy}\nabla\delta\varepsilon_{xy}\mathrm{d}z + \int_{-h/2}^{h/2} \sigma^{(1)}_{yy}\nabla\delta\varepsilon_{yy}\mathrm{d}z\right)\mathrm{d}y\right]_0^a\\ &\quad + \left[\int_0^a \left(\int_{-h/2}^{h/2} \sigma^{(1)}_{xx}\nabla\delta\varepsilon_{xx}\mathrm{d}z + 2\int_{-h/2}^{h/2} \sigma^{(1)}_{xy}\nabla\delta\varepsilon_{xy}\mathrm{d}z + \int_{-h/2}^{h/2} \sigma^{(1)}_{yy}\nabla\delta\varepsilon_{yy}\mathrm{d}z\right)\mathrm{d}x\right]_0^b\end{aligned} \tag{16}$$

Herein the stress resultants are defined as

$$\begin{Bmatrix} N_{xx} \\ N_{yy} \\ N_{xy} \end{Bmatrix} = \int_{-h/2}^{h/2} \begin{Bmatrix} t_{xx} \\ t_{yy} \\ t_{xy} \end{Bmatrix} \mathrm{d}z, \qquad \begin{Bmatrix} M_{xx} \\ M_{yy} \\ M_{xy} \end{Bmatrix} = \int_{-h/2}^{h/2} \begin{Bmatrix} t_{xx} \\ t_{yy} \\ t_{xy} \end{Bmatrix} z\,\mathrm{d}z$$
$$\begin{Bmatrix} N_{xx}^{(1)} \\ N_{yy}^{(1)} \\ N_{xy}^{(1)} \end{Bmatrix} = \int_{-h/2}^{h/2} \begin{Bmatrix} \sigma_{xx}^{(1)} \\ \sigma_{yy}^{(1)} \\ \sigma_{xy}^{(1)} \end{Bmatrix} \mathrm{d}z, \qquad \begin{Bmatrix} M_{xx}^{(1)} \\ M_{yy}^{(1)} \\ M_{xy}^{(1)} \end{Bmatrix} = \int_{-h/2}^{h/2} \begin{Bmatrix} \sigma_{xx}^{(1)} \\ \sigma_{yy}^{(1)} \\ \sigma_{xy}^{(1)} \end{Bmatrix} z\,\mathrm{d}z \tag{17}$$

Substituting Eqs. (11) and (12) into Eq. (16), the moment relations in conjunction with the flexural rigidities of the orthotropic nanoplates become:

$$\begin{aligned}\delta U = {} & \int_A \left(N_{xx}\delta\frac{\partial^2 u}{\partial x^2} - M_{xx}\delta\frac{\partial^2 w}{\partial x^2} + N_{xy}\delta\frac{\partial u}{\partial y} + N_{xy}\delta\frac{\partial v}{\partial x} - 2M_{xy}\delta\frac{\partial^2 w}{\partial x\partial y} + N_{yy}\delta\frac{\partial^2 v}{\partial y^2} - M_{yy}\delta\frac{\partial^2 w}{\partial y^2}\right)\mathrm{d}A \\ & + \left[\int_0^b \left(N_{xx}^{(1)}\delta\frac{\partial^2 u}{\partial x^2} - M_{xx}^{(1)}\delta\frac{\partial^2 w}{\partial x^2} + N_{xy}^{(1)}\delta\frac{\partial v}{\partial y} + N_{xy}^{(1)}\delta\frac{\partial u}{\partial x} - 2M_{xy}^{(1)}\delta\frac{\partial^2 w}{\partial x\partial y} + N_{yy}^{(1)}\delta\frac{\partial^2 v}{\partial y^2} - M_{yy}^{(1)}\delta\frac{\partial^2 w}{\partial y^2}\right)\mathrm{d}y\right]_0^a \\ & + \left[\int_0^a \left(N_{xx}^{(1)}\delta\frac{\partial^2 u}{\partial x^2} - M_{xx}^{(1)}\delta\frac{\partial^2 w}{\partial x^2} + N_{xy}^{(1)}\delta\frac{\partial v}{\partial y} + N_{xy}^{(1)}\delta\frac{\partial u}{\partial x} - 2M_{xy}^{(1)}\delta\frac{\partial^2 w}{\partial x\partial y} + N_{yy}^{(1)}\delta\frac{\partial^2 v}{\partial y^2} - M_{yy}^{(1)}\delta\frac{\partial^2 w}{\partial y^2}\right)\mathrm{d}x\right]_0^b \end{aligned} \tag{18}$$

The virtual work done by applied forces is

$$\delta W = -\int_A \begin{pmatrix} \left(f_{xx}\dfrac{\partial w_0}{\partial x}\dfrac{\delta\partial w_0}{\partial x} + f_{xy}\left(\dfrac{\partial w_0}{\partial x}\dfrac{\delta\partial w_0}{\partial y} + \dfrac{\partial w_0}{\partial y}\dfrac{\delta\partial w_0}{\partial x}\right) + f_{yy}\dfrac{\partial w_0}{\partial y}\dfrac{\delta\partial w_0}{\partial y}\right) \\ -k_{\mathrm{W}}\delta w_0 + k_{\mathrm{G}}\left(\dfrac{\partial w_0}{\partial x}\dfrac{\delta\partial w_0}{\partial x} + \dfrac{\partial w_0}{\partial y}\dfrac{\delta\partial w_0}{\partial y}\right) - \dfrac{\partial c_{\mathrm{D}}}{\partial t}\delta w_0 \end{pmatrix} \mathrm{d}A \tag{19}$$

here in k_{W}, k_{G} and c_{D} represent the spring constant, the shear layer parameter, and the viscous damping constant, respectively.

Now the final term of Hamilton's variational method (the kinetic energy) of a Kirchhoff orthotropic plate can be measured by

$$\begin{aligned}\delta K = {} & \int_A \int_{-h/2}^{h/2} \rho(\dot{u}\delta\dot{u} + \dot{v}\delta\dot{v} + \dot{w}\delta\dot{w})\,\mathrm{d}z\,\mathrm{d}x\,\mathrm{d}y \\ = {} & \int_A \left[-I_0(\dot{u}\delta\dot{u} + \dot{v}\delta\dot{v} + \dot{w}\delta\dot{w}) + I_1\left(\frac{\partial\delta\dot{w}}{\partial x}\dot{u} + \frac{\partial\dot{w}}{\partial x}\delta\dot{u} + \frac{\partial\delta\dot{w}}{\partial y}\dot{v} + \frac{\partial\dot{w}}{\partial y}\delta\dot{v}\right)\right. \\ & \left. - I_2\left(\frac{\partial\dot{w}}{\partial x}\frac{\partial\delta\dot{w}}{\partial x} + \frac{\partial\dot{w}}{\partial y}\frac{\partial\delta\dot{w}}{\partial y}\right)\right]\mathrm{d}x\,\mathrm{d}y \end{aligned} \tag{20}$$

in which ρ is the mass density and the mass moments of inertia are given by

$$\begin{Bmatrix} I_0 \\ I_1 \\ I_2 \end{Bmatrix} = \int_{-h/2}^{h/2} \rho \begin{Bmatrix} 1 \\ z \\ z^2 \end{Bmatrix} \mathrm{d}z\,\mathrm{d}A \tag{21}$$

According to the fundamental equations of Kirchhoff plate theory considering visco-Pasternak foundation, hygrothermal environment, and mechanical load, the equilibrium equations regarding the displacements for orthotropic plates using Hamilton's principle can be defined as:

$$\begin{aligned} & \delta u\colon \frac{\partial N_{xx}}{\partial x} + \frac{\partial N_{xy}}{\partial y} = I_0\frac{\partial^2 u}{\partial t^2} - I_1\frac{\partial^2}{\partial t^2}\left(\frac{\partial w}{\partial x}\right) \\ & \delta v\colon \frac{\partial N_{xy}}{\partial x} + \frac{\partial N_{yy}}{\partial y} = I_0\frac{\partial^2 v}{\partial t^2} - I_1\frac{\partial^2}{\partial t^2}\left(\frac{\partial w}{\partial y}\right) \\ & \delta w\colon \frac{\partial^2 M_{xx}}{\partial x^2} + 2\frac{\partial^2 M_{xy}}{\partial x\partial y} + \frac{\partial^2 M_{yy}}{\partial y^2} = f_{xx}\frac{\partial^2 w_0}{\partial x^2} + 2f_{xy}\frac{\partial^2 w_0}{\partial x\partial y} + f_{yy}\frac{\partial^2 w_0}{\partial y^2} + k_{\mathrm{W}}w_0 \\ & \qquad - k_{\mathrm{G}}\left(\frac{\partial^2 w_0}{\partial x^2} + \frac{\partial^2 w_0}{\partial y^2}\right) + c_{\mathrm{D}}\frac{\partial w_0}{\partial t} + I_0\frac{\partial^2 w}{\partial t^2} - I_2\frac{\partial^2}{\partial t^2}\left(\frac{\partial^2 w}{\partial x^2} + \frac{\partial^2 w}{\partial y^2}\right) + I_1\frac{\partial^2}{\partial t^2}\left(\frac{\partial u}{\partial x} + \frac{\partial v}{\partial y}\right) \end{aligned} \tag{22}$$

According to Eq. (18), the following classical and non-classical boundary conditions will be obtained as follows:

- classical boundary conditions

$$\begin{aligned}
&\text{At } x=0 \text{ or } a \qquad N_{xx} \text{ or } u, \qquad N_{xy} \text{ or } v, \qquad M_{xx} \text{ or } \frac{\partial w}{\partial x}, \qquad \frac{\partial M_{xx}}{\partial x}-2M_{xy}\frac{\partial w}{\partial x} \text{ or } w\\
&\text{At } y=0 \text{ or } b \qquad N_{yy} \text{ or } v, \qquad N_{xy} \text{ or } u, \qquad M_{yy} \text{ or } \frac{\partial w}{\partial y}, \qquad \frac{\partial M_{yy}}{\partial y}+2M_{xy}\frac{\partial w}{\partial x} \text{ or } w
\end{aligned} \tag{23}$$

- non-classical boundary conditions

$$\begin{aligned}
&\text{At } x=0 \text{ or } a \qquad N_{xx}^{(1)} \text{ or } \frac{\partial u}{\partial x}, \qquad M_{xx}^{(1)} \text{ or } \frac{\partial^2 w}{\partial x^2}, \qquad N_{yy}^{(1)} \text{ or } \frac{\partial v}{\partial y}\\
&\text{At } y=0 \text{ or } b \qquad N_{yy}^{(1)} \text{ or } \frac{\partial^2 w}{\partial y^2}, \qquad N_{xy}^{(1)} \text{ or } \frac{\partial u}{\partial y}+\frac{\partial v}{\partial x}, \qquad M_{xy}^{(1)} \text{ or } \frac{\partial^2 w}{\partial x \partial y}
\end{aligned} \tag{24}$$

Due to the higher-order nonlocal strain gradient theory, the equations of motion for a size-dependent rectangular nanoplate can be obtained as:

$$\begin{aligned}
N_{xx} &= (\mu_0^2+\mu_1^2)\nabla^2 N_{xx}-\mu_0^2\mu_1^2\nabla^4 N_{xx}+(1-\mu_1^2\nabla^2)\left(A_{11}\frac{\partial u}{\partial x}+A_{12}\frac{\partial v}{\partial y}\right)\\
&\quad -l^2(1-\mu_0^2\nabla^2)\nabla^2\left(A_{11}\frac{\partial u}{\partial x}+A_{12}\frac{\partial v}{\partial y}\right)\\
N_{yy} &= (\mu_0^2+\mu_1^2)\nabla^2 N_{yy}-\mu_0^2\mu_1^2\nabla^4 N_{yy}+(1-\mu_1^2\nabla^2)\left(A_{21}\frac{\partial u}{\partial x}+A_{22}\frac{\partial v}{\partial y}\right)\\
&\quad -l^2(1-\mu_0^2\nabla^2)\nabla^2\left(A_{21}\frac{\partial u}{\partial x}+A_{22}\frac{\partial v}{\partial y}\right)\\
N_{xy} &= (\mu_0^2+\mu_1^2)\nabla^2 N_{xy}-\mu_0^2\mu_1^2\nabla^4 N_{xy}+(1-\mu_1^2\nabla^2)\left(A_{66}\frac{\partial u}{\partial x}+A_{66}\frac{\partial v}{\partial y}\right)\\
&\quad -l^2(1-\mu_0^2\nabla^2)\nabla^2\left(A_{66}\frac{\partial u}{\partial x}+A_{66}\frac{\partial v}{\partial y}\right)
\end{aligned} \tag{25}$$

$$\begin{aligned}
M_{xx} &= (\mu_0^2+\mu_1^2)\nabla^2 M_{xx}-\mu_0^2\mu_1^2\nabla^4 M_{xx}-(1-\mu_1^2\nabla^2)\left(D_{11}\frac{\partial^2 w}{\partial x^2}+D_{12}\frac{\partial^2 w}{\partial y^2}\right)\\
&\quad +l^2(1-\mu_0^2\nabla^2)\nabla^2\left(D_{11}\frac{\partial^2 w}{\partial x^2}+D_{12}\frac{\partial^2 w}{\partial y^2}\right)\\
M_{yy} &= (\mu_0^2+\mu_1^2)\nabla^2 M_{yy}-\mu_0^2\mu_1^2\nabla^4 M_{yy}-(1-\mu_1^2\nabla^2)\left(D_{21}\frac{\partial^2 w}{\partial x^2}+D_{22}\frac{\partial^2 w}{\partial y^2}\right)\\
&\quad +l^2(1-\mu_0^2\nabla^2)\nabla^2\left(D_{21}\frac{\partial^2 w}{\partial x^2}+D_{22}\frac{\partial^2 w}{\partial y^2}\right)\\
M_{xy} &= (\mu_0^2+\mu_1^2)\nabla^2 M_{xy}-\mu_0^2\mu_1^2\nabla^4 M_{xy}-2(1-\mu_1^2\nabla^2)\left(D_{66}\frac{\partial^2 w}{\partial x \partial y}\right)\\
&\quad +2l^2(1-\mu_0^2\nabla^2)\nabla^2\left(D_{66}\frac{\partial^2 w}{\partial x \partial y}\right)
\end{aligned} \tag{26}$$

In the case of an orthotropic nanoplate, we have:

$$\begin{aligned}
&A_{11}=\frac{E_1 h}{1-\nu_{12}\nu_{21}}, \qquad A_{12}=\frac{\nu_{12}E_2 h}{1-\nu_{12}\nu_{21}}, \qquad A_{22}=\frac{E_2 h}{1-\nu_{12}\nu_{21}} A_{66}=G_{12}h\\
&D_{11}=\frac{E_1 h^3}{12(1-\nu_{12}\nu_{21})}, \qquad D_{12}=\frac{\nu_{12}E_2 h^3}{12(1-\nu_{12}\nu_{21})}, \qquad D_{22}=\frac{E_2 h^3}{12(1-\nu_{12}\nu_{21})}, \qquad D_{66}=\frac{G_{12}h^3}{12}
\end{aligned} \tag{27}$$

Substituting Eqs. (25) and (26) into Eq. (22) leads to

$$\begin{aligned}
\frac{\partial N_{xx}}{\partial x}+\frac{\partial N_{xy}}{\partial y} &= (\mu_0^2+\mu_1^2)\nabla^2\left(\frac{\partial N_{xx}}{\partial x}+\frac{\partial N_{xy}}{\partial y}\right)-\mu_0^2\mu_1^2\nabla^4\left(\frac{\partial N_{xx}}{\partial x}+\frac{\partial N_{xy}}{\partial y}\right)\\
&\quad +(1-\mu_1^2\nabla^2)\left(A_{11}\frac{\partial^2 u_0}{\partial x^2}+A_{12}\frac{\partial^2 v_0}{\partial x \partial y}+A_{66}\left(\frac{\partial^2 u_0}{\partial y^2}\frac{\partial^2 v_0}{\partial x \partial y}\right)\right)
\end{aligned}$$

$$-l^2(1-\mu_0^2\nabla^2)\nabla^2\left(A_{11}\frac{\partial^2 u_0}{\partial x^2}+A_{12}\frac{\partial^2 v_0}{\partial x\partial y}+A_{66}\left(\frac{\partial^2 u_0}{\partial y^2}\frac{\partial^2 v_0}{\partial x\partial y}\right)\right) \tag{28}$$

$$\begin{aligned}\frac{\partial N_{yy}}{\partial y}+\frac{\partial N_{xy}}{\partial x}&=(\mu_0^2+\mu_1^2)\nabla^2\left(\frac{\partial N_{yy}}{\partial y}+\frac{\partial N_{xy}}{\partial x}\right)-\mu_0^2\mu_1^2\nabla^4\left(\frac{\partial N_{yy}}{\partial y}+\frac{\partial N_{xy}}{\partial x}\right)\\&+(1-\mu_1^2\nabla^2)\left(A_{21}\frac{\partial^2 u_0}{\partial x\partial y}+A_{22}\frac{\partial^2 v_0}{\partial y^2}+A_{66}\left(\frac{\partial^2 u_0}{\partial x\partial y}\frac{\partial^2 v_0}{\partial x^2}\right)\right)\\&-l^2(1-\mu_0^2\nabla^2)\nabla^2\left(A_{21}\frac{\partial^2 u_0}{\partial x\partial y}+A_{22}\frac{\partial^2 v_0}{\partial y^2}+A_{66}\left(\frac{\partial^2 u_0}{\partial x\partial y}\frac{\partial^2 v_0}{\partial x^2}\right)\right)\end{aligned} \tag{29}$$

$$\begin{aligned}&\frac{\partial^2 M_{xx}}{\partial x^2}+2\frac{\partial^2 M_{xy}}{\partial x\partial y}+\frac{\partial^2 M_{yy}}{\partial y^2}\\&=(\mu_0^2+\mu_1^2)\nabla^2\left(\frac{\partial^2 M_{xx}}{\partial x^2}+2\frac{\partial^2 M_{xy}}{\partial x\partial y}+\frac{\partial^2 M_{yy}}{\partial y^2}\right)-\mu_0^2\mu_1^2\nabla^4\left(\frac{\partial^2 M_{xx}}{\partial x^2}+2\frac{\partial^2 M_{xy}}{\partial x\partial y}+\frac{\partial^2 M_{yy}}{\partial y^2}\right)\\&-(1-\mu_1^2\nabla^2)\left(D_{11}\frac{\partial^4 w_0}{\partial x^4}+D_{12}\frac{\partial^4 w_0}{\partial x^2\partial y^2}+4D_{66}\frac{\partial^4 w_0}{\partial x^2\partial y^2}+D_{21}\frac{\partial^4 w_0}{\partial x^2\partial y^2}+D_{22}\frac{\partial^4 w_0}{\partial y^4}\right)\\&+l^2(1-\mu_0^2\nabla^2)\nabla^2\left(D_{11}\frac{\partial^4 w_0}{\partial x^4}+D_{12}\frac{\partial^4 w_0}{\partial x^2\partial y^2}+4D_{66}\frac{\partial^4 w_0}{\partial x^2\partial y^2}+D_{21}\frac{\partial^4 w_0}{\partial x^2\partial y^2}+D_{22}\frac{\partial^4 w_0}{\partial y^4}\right)\end{aligned} \tag{30}$$

Using Eq. (22) and Eqs. (29)–(30), the equations of motion for a size-dependent rectangular nanoplate based on the higher-order nonlocal strain gradient theory can be determined as

$$\begin{aligned}&(1-\mu_0^2\nabla^2-\mu_1^2\nabla^2+\mu_0^2\mu_1^2\nabla^4)\left(I_0\frac{\partial^2 u_0}{\partial t^2}-I_1\frac{\partial^3 w_0}{\partial t^2\partial x}\right)\\&=((1-\mu_1^2)-l^2(1-\mu_0^2)\nabla^2)\left(A_{11}\frac{\partial^2 u}{\partial x^2}+A_{12}\frac{\partial^2 v}{\partial x\partial y}+A_{66}\left(\frac{\partial^2 u}{\partial y^2}+\frac{\partial^2 v}{\partial x\partial y}\right)\right)\end{aligned} \tag{31}$$

$$\begin{aligned}&(1-\mu_0^2\nabla^2-\mu_1^2\nabla^2+\mu_0^2\mu_1^2\nabla^4)\left(I_0\frac{\partial^2 v_0}{\partial t^2}-I_1\frac{\partial^3 w_0}{\partial t^2\partial x}\right)\\&=((1-\mu_1^2)-l^2(1-\mu_0^2)\nabla^2)\left(A_{21}\frac{\partial^2 u}{\partial x\partial y}+A_{22}\frac{\partial^2 v}{\partial y^2}+A_{66}\left(\frac{\partial^2 u}{\partial x\partial y}+\frac{\partial^2 v}{\partial x^2}\right)\right)\end{aligned} \tag{32}$$

$$\begin{aligned}&(1-\mu_0^2\nabla^2-\mu_1^2\nabla^2+\mu_0^2\mu_1^2\nabla^4)\left(I_0\frac{\partial^2 w_0}{\partial t^2}-I_2\frac{\partial^2}{\partial t^2}\left(\frac{\partial^2 w_0}{\partial x^2}+\frac{\partial^2 w_0}{\partial y^2}\right)+I_1\frac{\partial^2}{\partial t^2}\left(\frac{\partial u_0}{\partial x}+\frac{\partial v_0}{\partial y}\right)\right)\\&=((1-\mu_1^2)-l^2(1-\mu_0^2)\nabla^2)\left(-D_{11}\frac{\partial^4 w}{\partial x^4}-D_{12}\frac{\partial^4 w}{\partial x^2\partial y^2}-4D_{66}\frac{\partial^4 w}{\partial x^2\partial y^2}-D_{21}\frac{\partial^4 w}{\partial x^2\partial y^2}\right.\\&\left.-D_{22}\frac{\partial^4 w}{\partial y^4}\right)+(1-\mu_0^2\nabla^2-\mu_1^2\nabla^2+\mu_0^2\mu_1^2\nabla^4)\left(-k_W+k_G\left(\frac{\partial^2 w_0}{\partial x^2}+\frac{\partial^2 w_0}{\partial y^2}\right)-c_D\frac{\partial w_0}{\partial t}\right)\end{aligned} \tag{33}$$

Regarding the above equations [i.e., Eqs. (31)–(33)], it can be found that the equation of in-plane displacements is not coupled with aligning equations of transverse displacement. Hence, we only select Eq. (33) to study the transverse vibration problem. Furthermore, when neglecting the rotary inertia (I_2 and I_1), the governing equation of viscoelastic orthotropic nanoplates based upon the higher-order nonlocal strain gradient theory can be expressed as:

$$\begin{aligned}&\left(1+g\frac{\partial}{\partial t}\right)\left\{(1-\mu_0\nabla^2-l\nabla^2+l\mu_0\nabla^4)\left\{D_{11}\frac{\partial^4 w_0}{\partial x^4}+(2D_{12}+4D_{66})\frac{\partial^4 w_0}{\partial x^2\partial y^2}+D_{22}\frac{\partial^4 w_0}{\partial y^4}\right\}\right\}\\&+(1-\mu_0\nabla^2-\mu_1\nabla^2+\mu_0\mu_1\nabla^4)\left\{(f_{xx}+k_G)\frac{\partial^2 w_0}{\partial x^2}+(f_{yy}+k_G)\frac{\partial^2 w_0}{\partial y^2}+2f_{xy}\frac{\partial^2 w_0}{\partial x\partial y}-I_0\frac{\partial^2 w_0}{\partial t^2}\right.\\&\left.-\left(k_W+c_D\frac{\partial}{\partial t}\right)w_0\right\}=0\end{aligned} \tag{34}$$

3.3. Solution methodology

In this subsection, an analytical solution will be presented for the free vibration of a simply-supported Kirchhoff nanoplate using the higher-order nonlocal strain gradient theory. By applying Eqs. (23) and (24), we will have the classical and non-classical boundary conditions of a simply supported Kirchhoff nanoplate as follows:

Table 1
Geometrical and temperature-dependent material properties of single-layer graphene sheets.

h (nm)	a (nm)	b (nm)	E_1 (TPa)	E_2 (TPa)	G_{12} (TPa)	ν_{12}	ρ (kg/m^3)	α_{11} (10^{-6}/K)	α_{22} (10^{-6}/K)	β_{11} (wt.% H_2O)$^{-1}$	β_{22} (wt.% H_2O)$^{-1}$
0.156	4.888	4.855	1.949	1.962	0.846	0.201	5295	1.9	2.1	0.0026	0.0

Classical boundary conditions	Non-classical boundary conditions
$M_{xx}(0,y,t) = M_{xx}(a,y,t) = 0$	$\dfrac{\partial^2 w(0,y,t)}{\partial x^2} = \dfrac{\partial^2 w(a,y,t)}{\partial x^2} = 0$
$w(0,y,t) = w(a,y,t) = 0$	$\dfrac{\partial^2 w(0,y,t)}{\partial y^2} = \dfrac{\partial^2 w(a,y,t)}{\partial y^2} = 0$
$M_{yy}(x,0,t) = M_{yy}(x,b,t) = 0$	$\dfrac{\partial^2 w(x,0,t)}{\partial x^2} = \dfrac{\partial^2 w(x,b,t)}{\partial x^2} = 0$
$w(x,0,t) = w(x,b,t) = 0$	$\dfrac{\partial^2 w(x,0,t)}{\partial y^2} = \dfrac{\partial^2 w(x,b,t)}{\partial y^2} = 0$

(35)

The following expansion of the displacement field may be considered for consideration of simply supported boundary conditions in rectangular nanoplates,

$$u_z(x,y,t) = \sum_{m=1}^{\infty}\sum_{n=1}^{\infty} w \sin(\alpha x)\sin(\beta y)\mathrm{e}^{\lambda(m,n)t} \tag{36}$$

in which λ is the complex eigenfrequency associated with the (m, n)-th eigenmode, and $\alpha = m\pi/a$, $\beta = n\pi/b$. Also, w is an unknown coefficient to be determined.

By substituting Eq. (26) into Eq. (25), the equation of motion can be summarized as a matrix form as follows,

$$\left[K + C\lambda(m,n) + M\lambda^2(m,n)\right]w = 0 \tag{37}$$

or

$$\left[\omega_0^2 + 2\xi\omega_0\lambda(m,n) + \lambda^2(m,n)\right]w = 0 \tag{38}$$

where the undamped frequency ω_0 and the damping ratio ξ are given by

$$\omega_0 = \sqrt{\frac{K}{M}}, \qquad \xi = \frac{C}{\sqrt{4KM}} \tag{39}$$

here K, M, and C are, respectively, mass, stiffness, and damping coefficients, and can be seen in Appendix A. The (m,n)-th order of the complex eigenfrequency corresponding to the viscoelastic orthotropic nanoplates can be obtained analytically as

$$\lambda(m,n) = \frac{-C \pm \mathrm{i}\sqrt{4KM - C^2}}{2M} \tag{40}$$

here $\mathrm{i} = \sqrt{-1}$. Note that K, M, and C have been defined in Appendix A. It should be noted [69] that its real part can give a measure (or an index) of the rate of decay (or divergence) of the vibrational mode, and the imaginary part of the complex eigenfrequency gives a measure (or an index) of the rate of oscillation of the considered structures. Noting that, the vibration of the nanoplate is under-damped if $0 < \xi < 1$, critically-damped if $\xi = 1$, and over-damped if $\xi > 1$. The complex eigenfrequency has become an integral part of many applications, including an index for measuring the role of damping on dynamic responses or determining the stability of structural systems when they contain some sources of energy such as hygrothermal environment, and fluid components [70].

4. Results and discussion

Numerical results are presented in this section for the hygro-thermo-viscoelastic vibration of simply supported viscoelastic orthotropic SLGS resting on a visco-Pasternak foundation. To achieve this aim, the effective material properties of SLGS and belongings should be specified first. Hence, the material properties, the geometries as well as the thermal expansion coefficients for SLGS were taken from MD simulation results [15] and the coefficients of moisture expansions have been adapted from analytical models [58,71,72] that are listed in Table 1. Moreover, SLGS looks like a sheet containing honeycomb carbon atoms and its efficiency is dependent on the atomic structure. In order to present the numerical results in the forms of graphical and tabular, some dimensionless parameters are defined for natural frequencies and components of the visco-Pasternak foundation [62]:

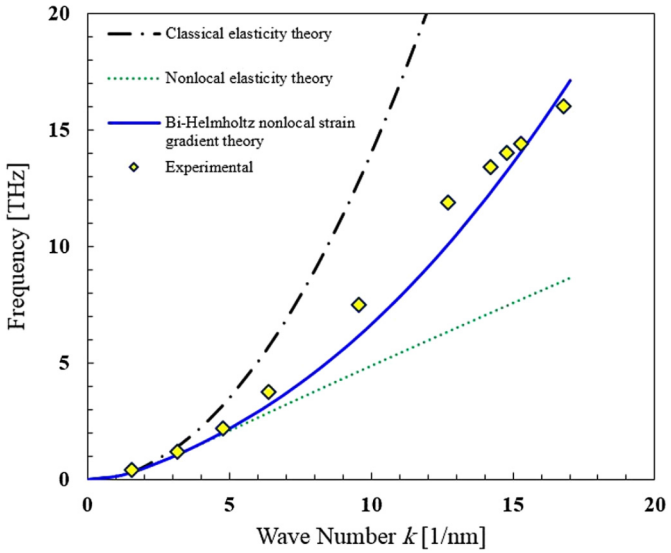

Fig. 2. Wave characteristics of SLGS according to the experimental data, the nonlocal elasticity model [15], the classical elasticity model, and the bi-Helmholtz nonlocal strain-gradient model (the lower-order nonlocal parameter $\mu_0 = 0.34$ nm, the higher-order nonlocal parameter $\mu_1 = 0.54$ nm, and the material characteristic parameter $l = 0.21$ nm).

Table 2
Natural frequencies (in GHz) of SLGS in thermal environment.

Model	ΔT (K)		
	0	100	200
MD simulation [15]	114.4	–	–
Nonlocal elasticity model [15]	114.4[a]	105.7[a]	94.7[a]
Bi-Helmholtz nonlocal strain-gradient model	114.44[b]	105.54[b]	95.86[b]

Superscript a and b identify the small-scale parameters, a: $\mu_0 = 0.27$ nm, $\mu_1 = 0$, $l = 0$, b: $\mu_0 = 0.34$ nm, $\mu_1 = 0.54$ nm, $l = 0.21$nm.

$$\bar{\lambda} = \lambda a^2 \sqrt{\frac{\rho h}{D_{11}}}, \qquad \mathrm{K_W} = \frac{k_W a^4}{D_{11}}, \qquad \mathrm{K_G} = \frac{k_G a^2}{D_{11}}, \qquad \mathrm{C_D} = \frac{c_D a^2}{\sqrt{\rho h D_{11}}}, \qquad \mathrm{G} = \frac{g}{a^2}\sqrt{\frac{D_{11}}{\rho h}} \tag{41}$$

4.1. Identifying nonlocal and material characteristic parameters and comparison studies

In the exact analysis of graphene, often the optimal small-scale parameters are reported from atomic lattice dynamics, MD simulation or experimental data by matching the wave dispersion relation and frequency. In this field, Shen et al. [15] identified the optimal nonlocal parameter for the free-vibration frequency of simply supported SLGS using nonlocal elasticity theory by matching results with the MD simulation. As mentioned in the introduction section, the capacity of nonlocal elasticity theory to satisfy other size-dependent effects on the mechanical properties of nanoscale structures may lead to some limited problems [32,73]. Hence, the dispersion relation between wave frequency and wave number of SLGS was investigated by employing nonlocal strain gradient theory (NSGT) and the experimental data [34,74]. In their work, with identified small-scale parameters, the results were close to experimental data for the only wave behavior. Now, by adopting bi-Helmholtz nonlocal strain gradient theory (bi-H NSGT) as a size-dependent theory including three small-scale parameters, the optimal lower and higher order nonlocal parameters related to nonlocal effect, and material characteristic parameter related to strain gradient effect will be identified for SLGS. The benefit of the proposed model is compared with both experimental data [75] and MD simulation [15], as shown in Fig. 2 and Table 2.

The flexural frequency as a function of wave number for SLGS is drawn in Fig. 2. Our results on basis of bi-H NSGT with the identified small-scale parameters ($\mu_0 = 0.34$ nm, $\mu_1 = 0.54$ nm, $l = 0.21$ nm) are included in Fig. 2. The experimental data [75] and results obtained by nonlocal elasticity theory (the nonlocal parameter was fixed by MD simulation [15]) and classical elasticity theory (CET) are also computed and figured for comparison. As shown, the frequency curves calculated by CET, nonlocal elasticity theory (NET) [15], and bi-H NSGT almost match with experimental data [75] when the wave number is less than around 1 (1/nm). It means that, in small wave numbers [$k < 1$ (1/nm)], all the three continuum theories can give agreeable results. This is because the properties frequency of nanostructures (such as graphene) has not permeability to its frequency when the low wave numbers [$k < 1$ (1/nm)] are considered. However, when one considers wave numbers larger than 1 (1/nm), only bi-H NSGT is reliable for frequency. This is due to the fact, with an increment in wave number,

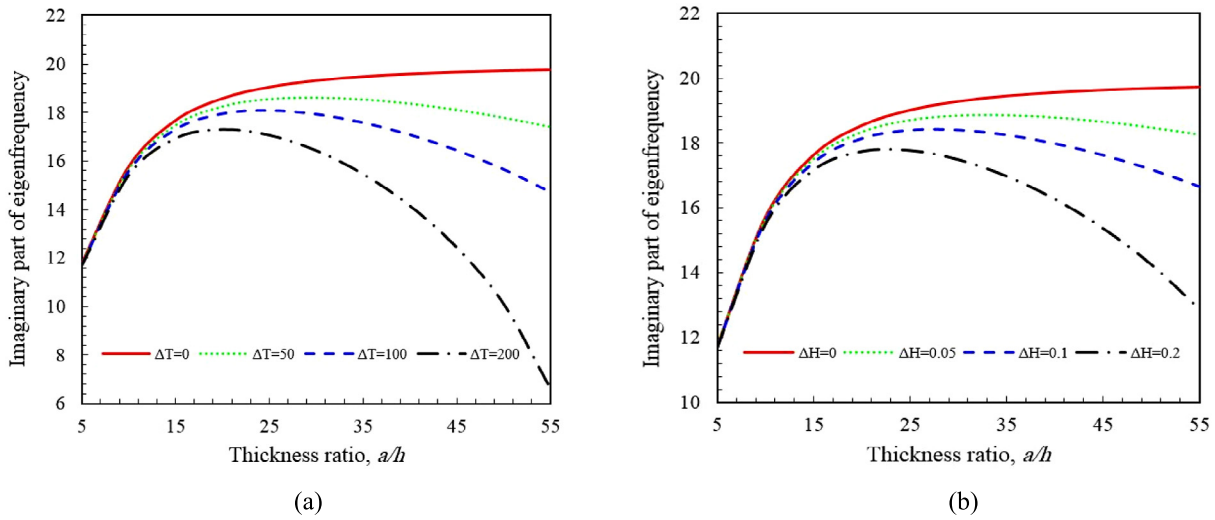

Fig. 3. Influence of **a)** a temperature rise and **b)** a moisture rise on the frequency of simply supported SLGS.

that the dependence of wave frequency on material properties and size effects (such like softening-stiffness effect and the stiffness-enhancement effect) will be more important. Accordingly, it can be found that in high wave numbers, the supplementary small-scale parameters need to be considered to reach results with a sufficient accuracy.

As can be observed in Table 2, using the identified small-scale parameters on the basis of bi-H NSGT leads to a good agreement between MD simulation [15] and the results obtained by nonlocal elasticity theory [15] in the absence and presence of thermal environment for the frequency of simply supported SLGS.

4.2. Case studies

Hereinafter, the geometry of SLGS are fixed at $a = b = j \times h$, for $(j = 5, 10, 20, \ldots, 55)$, the material properties, and the identified small-scale parameters will be used to analyze the role of parameters as temperature and moisture rise of the environment, structural damping, and hardness of elastic and viscoelastic foundations on the free vibration of simply supported SLGS.

4.2.1. Effect of temperature and moisture rise

The influence of temperature and moisture rise on the vibration behavior of SLGS for various thickness ratios is studied in Fig. 3.

As shown in Fig. 3,

1) the existence of an environmental condition decreases the frequency of graphene sheet,
2) the impact of moisture rise on the eigenfrequency is more sensitive than that of temperature rise,
3) an environmental condition is more influential in the higher values of the thickness ratios,
4) in the absence of an environmental condition, the frequency is increased with the increment in thickness ratio. However, in the presence of temperature or moisture environment, with increasing the thickness ratio of the graphene sheet, the imaginary part of the frequency rises to its peak, and then decreases. That is, the frequency of the nanoplate has case sensitivity to the variation of thickness ratio in the presence of a hygrothermal environment.

4.2.2. Effect of structural damping coefficient

The complex frequency of the viscoelastic SLGS due to changes in the structural damping coefficient (G) for diverse ranges of thickness ratio is studied in Fig. 4.

We can see that the regions in which $\xi > 1$, $\xi = 1$, and $\xi < 1$ for different structural damping coefficients are in Fig. 4a. According to Fig. 4,

1) the imaginary part of the eigenfrequency reduces by raising the value of the structural damping coefficient, and in the following, it reaches zero when the SLGS is critically-damped ($\xi = 1$),
2) the real part of the eigenfrequency has a divergence behavior when damping exceeds a critically-damped point,
3) when considering a constant structural damping coefficient, the increase in thickness ratio leads to an increasing damping ratio,
4) in the presence of a structural damping coefficient, a thinner graphene has a larger damping capacity.

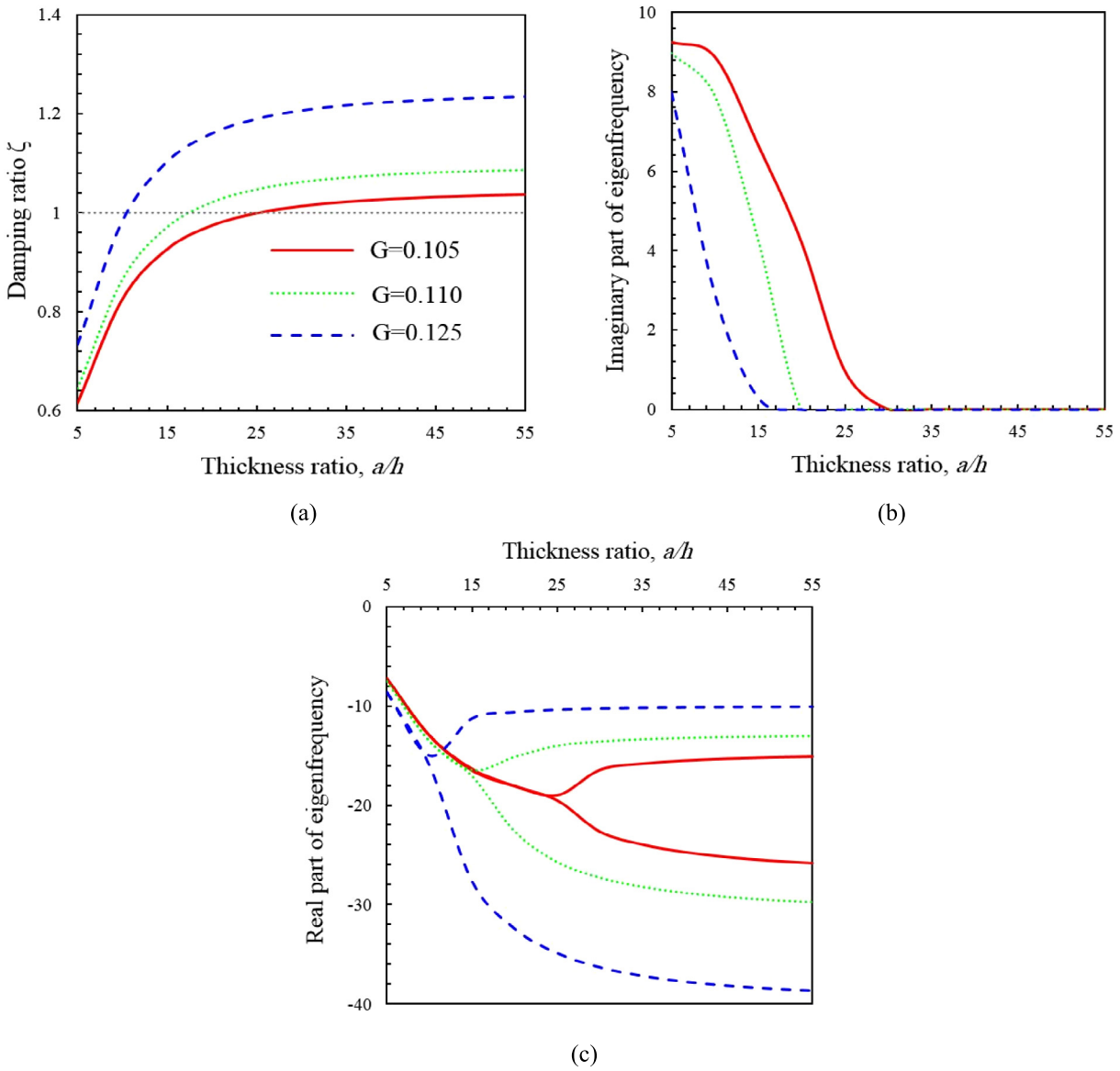

Fig. 4. Complex frequency of simply supported SLGS due to the variation of the structural damping coefficient.

4.2.3. Effect of viscous damping constant

The complex frequency responses of SLGS for diverse ranges of viscous damping constant due to the variation of the thickness ratio is plotted in Fig. 5. As observed from Fig. 5, with the increment in the viscous damping constant, energy absorption is increased, and the system tends to an overdamped system. Additionally, in the case of the high values of the viscous damping constant, the responsibility of the thickness ratio in the progress of the imaginary and real parts of the eigenfrequency is different. In the presence of a viscous damping constant, a thicker graphene has a larger damping capacity.

4.2.4. Effect of elastic and viscoelastic foundations in various conditions

According to bi-H NSGT, the remarkable effects of different elastic and visco-state foundations on the complex eigenfrequency of SLGS are exhibited in Table 3.

1) Foundation raises the eigenfrequency of the SLGS. This increment is in connection with the hardness effect of chosen foundation. Hence, a SLGS with foundations tends to a stiffer structure than that without a foundation.
2) The Pasternak foundation due to the consideration of an extra shear layer for illustrating transverse loads is more effective than the Winkler one in order to increase the imaginary part of the eigenfrequency.

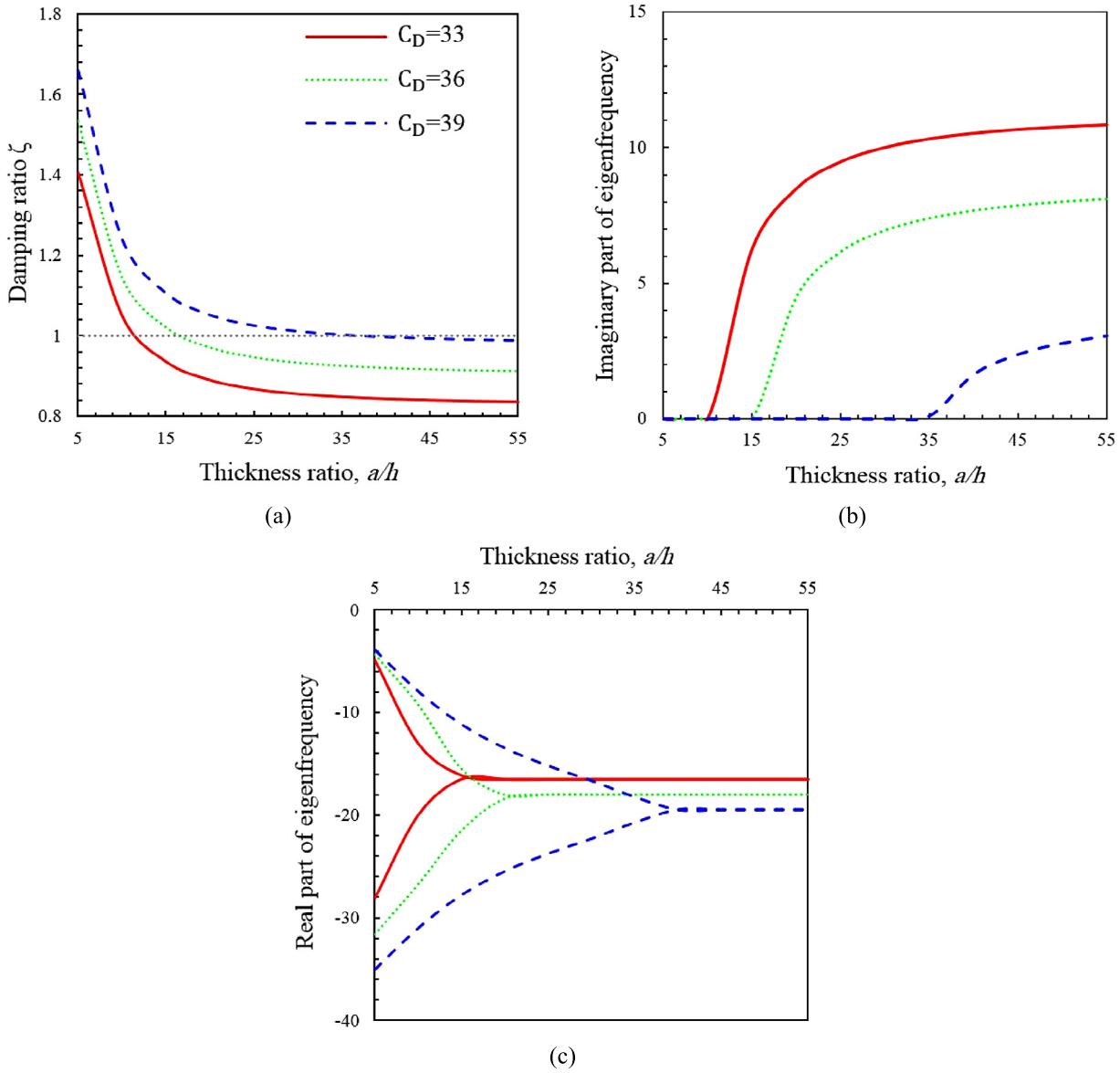

Fig. 5. Complex frequency of simply supported SLGS due to the variation of the structural damping coefficient.

3) The visco-state supposition of the foundation decreases the imaginary part of the eigenfrequency while it leads to a higher real part in eigenfrequency at the same time. These are due to the fact that visco-state makes the medium rough. Roughness is related to the influence of extra damping loads that exists in this type of foundation due to the practical use of the recoverable reserves in the system.
4) The presence of moisture and temperature rise leads to a considerable reduction in the eigenfrequency of the elastic orthotropic graphene. Moreover, it is observed that the power of the environment condition to decrease the eigenfrequency at higher values of the thickness ratio is larger than for the lower ones.
5) Another important observation is that with considering the structural damping coefficient (viscoelastic distribution of material properties), the absorption of energy is increased.

4.2.5. Effect of mode numbers

By considering the constant temperature and moisture values as well as constant visco-Pasternak foundation, the graphical relationships between the structural damping coefficient and the higher-order frequency parameters of graphene based on CET, nonlocal elasticity theory (NET), and bi-H NSGT are plotted in Fig. 6 for a constant thickness ratio ($a/h = 10$). As shown in Fig. 6, with the increment in structural damping coefficient, distinct size-dependent continuum theories have different trends of reaction in the higher modes of the imaginary part of the eigenfrequency. The eigenfrequency curves

Table 3
Comprehensive study of the complex eigenfrequency of elastic and viscoelastic SLGS due to varying foundation types and environmental conditions. ($\mu_0 = 0.34$ nm, $\mu_1 = 0.54$ nm, $l = 0.21$ nm, $G = 0.05$, $\Delta T = 200$, $\Delta H = 0.1$, $K_W = 200$, $K_G = 20$, $C_D = 5$).

	a/h	Type of foundation	No environment	Thermal environment	Hygrothermal environment
Elastic	10	Without foundation	$\pm 15.723\,i$	$\pm 15.355i$	$\pm 15.234i$
		Winkler foundation	$\pm 21.147\,i$	$\pm 20.875i$	$\pm 20.786i$
		Pasternak foundation	$\pm 29.017i$	$\pm 28.819i$	$\pm 28.755i$
		Visco-Winkler foundation	$-2.500 \pm 20.999i$	$-2.500 \pm 20.725i$	$-2.500 \pm 20.636i$
		Visco-Pasternak foundation	$-2.500 \pm 28.909i$	$-2.500 \pm 28.711i$	$-2.500 \pm 28.646i$
	50	Without foundation	$\pm 19.698i$	$\pm 10.119i$	$\pm 3.135i$
		Winkler foundation	$\pm 24.249i$	$\pm 17.389i$	$\pm 14.486i$
		Pasternak foundation	$\pm 31.350i$	$\pm 26.404i$	$\pm 24.589i$
		Visco-Winkler foundation	$-2.500 \pm 24.120i$	$-2.500 \pm 17.209i$	$-2.500 \pm 14.268i$
		Visco-Pasternak foundation	$-2.500 \pm 31.250i$	$-2.500 \pm 26.285i$	$-2.500 \pm 24.462i$
Viscoelastic	10	Without foundation	$-6.180 \pm 14.457i$	$-6.180 \pm 14.056i$	$-6.180 \pm 13.924i$
		Winkler foundation	$-6.180 \pm 20.224i$	$-6.180 \pm 19.940i$	$-6.180 \pm 19.846i$
		Pasternak foundation	$-6.180 \pm 28.351i$	$-6.180 \pm 28.149i$	$-6.180 \pm 28.083i$
		Visco-Winkler foundation	$-8.680 \pm 19.284i$	$-8.680 \pm 18.985i$	$-8.680 \pm 18.887i$
		Visco-Pasternak foundation	$-8.680 \pm 27.688i$	$-8.680 \pm 27.481i$	$-8.680 \pm 27.414i$
	50	Without foundation	$-9.700 \pm 17.144i$	$-9.700 \pm 12.879i$	$-9.700 \pm 9.447i$
		Winkler foundation	$-9.700 \pm 22.224i$	$-9.700 \pm 14.432i$	$-9.700 \pm 10.758i$
		Pasternak foundation	$-9.700 \pm 29.811i$	$-9.700 \pm 24.558i$	$-9.700 \pm 22.595i$
		Visco-Winkler foundation	$-12.200 \pm 20.956i$	$-12.200 \pm 12.391i$	$-12.200 \pm 7.809i$
		Visco-Pasternak foundation	$-12.200 \pm 28.878i$	$-12.200 \pm 23.416i$	$-12.200 \pm 21.349i$

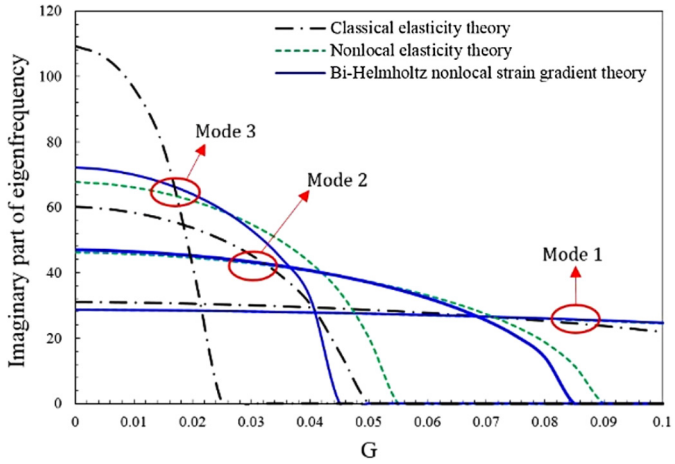

Fig. 6. Higher-order frequencies of simply supported SLGS with changes in the structural damping coefficient for various continuum theories ($G = 0.05$, $\Delta T = 200$, $\Delta H = 0.1$, $K_W = 200$, $K_G = 20$, $C_D = 5$).

calculated by CET, NET, and bi-H NSGT are close when the mode numbers (m, n) are equal to one. It indicates that, in the lower mode numbers, NET and bi-H NSGT can predict agreeable results. Although, when one considers mode numbers larger than one ($n > 1$), the NET and bi-H NSGT present different graphical trends for the eigenfrequency. Hence, it is required to consider supplementary small-scale parameters to achieve much accuracy, especially in higher mode numbers. In high-order mode, the viscosity of the material (the structural damping coefficient) has a superior role in the results and creates a sharpness of decline on the imaginary part of the eigenfrequency.

5. Conclusions

Damped vibration of simply-supported viscoelastic SLGS surrounded by visco-Pasternak foundation and exposed to the hygrothermal environment is studied analytically. The lower and higher order nonlocal parameters appraised the softening-stiffness effect in SLGS, whereas the material characteristic parameter appraised the stiffness-enhancement effect in SLGS. According to Kirchhoff plate theory in conjunction with the higher-order (bi-Helmholtz) nonlocal strain gradient theory, the equations of vibrational motion are derived using Hamilton's principle. The effects of various parameters on the vibration of SLGSs are investigated in detail. Based on our numerical results, the following conclusions can be notable:

- the developed model based on bi-H NSGT with the identified small-scale parameters ($\mu_0 = 0.34$ nm, $\mu_1 = 0.54$ nm, $l = 0.21$ nm) can reasonably interpret the softening effects of flexural frequencies of the SLGS, and shows a reasonably good match with the experimental flexural frequencies;
- the increase in the spring constant and the shear layer parameter will lead to increasing eigenfrequencies. However, the larger values of temperature, moisture, and structural damping coefficient will result in lower eigenfrequencies;
- the influence of environmental loading on the eigenfrequency increases with increasing the thickness ratio of the SLGS. However, the influence of elastic foundation on the eigenfrequency decreases with increasing the thickness ratio;
- in the case of a viscous damping constant, a thicker graphene has a larger damping capacity. However, for the case of a viscous damping constant, a thicker graphene has a larger damping capacity;
- the structural damping coefficient and the viscous damping constant have an important effect on the real part of eigenfrequency for the over-damped case, while both have a little effect on the real part of eigenfrequency for the under-damped case;
- the presence of elastic foundation leads to the increment in the stiffness and imaginary part of the eigenfrequency of the SLGS;
- the influence of small-scale parameters on the eigenfrequency will be more significant for higher-order modes.

Acknowledgements

Li Li acknowledges the supports of the National Natural Science Foundation of China (Grant No. 51605172), the Natural Science Foundation of Hubei Province of China (Grant No. 2016CFB191) and the Fundamental Research Funds for the Central Universities (Grant No. 2015MS014).

Appendix A

$$\begin{aligned}K &= \left\{D_{11}\alpha^4 + (2D_{12} + 4D_{66})\alpha^2\beta^2 + D_{22}\beta^4\right\} + (\mu_0 + l)\left\{D_{11}\alpha^6 + (D_{11} + 2D_{12} + 4D_{66})\alpha^4\beta^2\right.\\ &\quad \left. + (2D_{12} + D_{22} + 4D_{66})\alpha^2\beta^4 + D_{22}\alpha^6\right\} + l\mu_0\left\{D_{11}\alpha^8 + (D_{11} + 4D_{12} + 8D_{66} + D_{22})\alpha^4\beta^4 + D_{22}\beta^8\right.\\ &\quad \left. + (2D_{11} + 2D_{12} + 4D_{66})\alpha^6\beta^2 + (2D_{12} + 2D_{22} + 4D_{66})\alpha^2\beta^6\right\} - (f_{xx} + k_G)\alpha^2 + 2f_{xy}\alpha\beta\\ &\quad - (f_{yy} + k_P)\beta^2 - k_W - (\mu_0 + \mu_1)\left\{(f_{xx} + k_G)\alpha^4 + (f_{xx} + f_{yy} + 2k_G)\alpha^2\beta^2 + (f_{yy} + k_G)\beta^4\right.\\ &\quad \left. - 2f_{xy}\left(\alpha^3\beta + \alpha\beta^3\right) + k_W\left(\alpha^2 + \beta^2\right)\right\} - \mu_0\mu_1\left\{(f_{xx} + 2f_{yy} + k_G)\alpha^2\beta^4 + (f_{xx} + k_G)\alpha^6\right.\\ &\quad \left. + (2f_{xx} + f_{yy} + 2k_G)\alpha^4\beta^2 - (f_{yy} + k_G)\alpha^6 - 2f_{xy}\left(\alpha^5\beta + 2\alpha^3\beta^3 + \alpha\beta^5\right) + k_w\left(\alpha^4 + 2\alpha^4\beta^3 + \beta^4\right)\right\} \qquad (42)\end{aligned}$$

$$\begin{aligned}C &= g\left\{D_{11}\alpha^4 + (2D_{12} + 4D_{66})\alpha^2\beta^2 + D_{22}\beta^4 + (\mu_0 + l)\left\{D_{11}\alpha^6 + (D_{11} + 2D_{12} + 4D_{66})\alpha^4\beta^2\right.\right.\\ &\quad \left. + (2D_{12} + D_{22} + 4D_{66})\alpha^2\beta^4 + D_{22}\alpha^6\right\} + l\mu_0\left\{D_{11}\alpha^8 + (D_{11} + 4D_{12} + 8D_{66} + D_{22})\alpha^4\beta^4 + D_{22}\beta^8\right.\\ &\quad \left.\left. + (2D_{11} + 2D_{12} + 4D_{66})\alpha^6\beta^2 + (2D_{12} + 2D_{22} + 4D_{66})\alpha^2\beta^6\right\}\right\} + c_D\left\{\left(1 - (\mu_0 + \mu_1)\right)\left(\alpha^2 + \beta^2\right)\right.\\ &\quad \left. - \mu_0\mu_1\left(\alpha^4 + 2\alpha^2\beta^2 + \beta^4\right)\right\} \qquad (43)\end{aligned}$$

$$M = I_0\left(1 + (\mu_0 + \mu_1)\left(\alpha^2 + \beta^2\right) + \mu_0\mu_1\left(\alpha^4 + 2\alpha^2\beta^2 + \beta^4\right)\right) \qquad (44)$$

References

[1] C. Chen, J. Hone, Graphene nanoelectromechanical systems, Proc. IEEE 101 (7) (2013) 1766–1779.
[2] J. Schroeder, F.P. Cammisa, Carbon nanotubes and graphene patches and implants for biological tissue, 2014, Google Patents.
[3] K. Duan, et al., Pillared graphene as an ultra-high sensitivity mass sensor, Sci. Rep. 7 (1) (2017) 14012.
[4] J. Liang, et al., Electromechanical actuators based on graphene and graphene/Fe_3O_4 hybrid paper, Adv. Funct. Mater. 21 (19) (2011) 3778–3784.
[5] D.C. Lam, et al., Experiments and theory in strain gradient elasticity, J. Mech. Phys. Solids 51 (8) (2003) 1477–1508.
[6] E. Andrews, et al., Size effects in ductile cellular solids, part II: experimental results, Int. J. Mech. Sci. 43 (3) (2001) 701–713.
[7] G.-L. She, et al., Nonlinear bending and vibration analysis of functionally graded porous tubes via a nonlocal strain gradient theory, Compos. Struct. (2018).
[8] G.-L. She, et al., On buckling and postbuckling behavior of nanotubes, Int. J. Eng. Sci. 121 (2017) 130–142.
[9] D. Shahsavari, B. Karami, L. Li, A high-order gradient model for wave propagation analysis of porous FG nanoplates, Steel Compos. Struct. (2018), just-accepted.
[10] G.-L. She, F.-G. Yuan, Y.-R. Ren, Nonlinear analysis of bending, thermal buckling and post-buckling for functionally graded tubes by using a refined beam theory, Compos. Struct. 165 (2017) 74–82.
[11] B. Karami, D. Shahsavari, M. Janghorban, Wave propagation analysis in functionally graded (*FG*) nanoplates under in-plane magnetic field based on nonlocal strain gradient theory and four variable refined plate theory, Mech. Adv. Mat. Struct. 25 (12) (2018) 1047–1057.
[12] A.C. Eringen, D. Edelen, On nonlocal elasticity, Int. J. Eng. Sci. 10 (3) (1972) 233–248.
[13] J. Reddy, Nonlocal theories for bending, buckling and vibration of beams, Int. J. Eng. Sci. 45 (2–8) (2007) 288–307.
[14] M. Aydogdu, A general nonlocal beam theory: its application to nanobeam bending, buckling and vibration, Physica E, Low-Dimens. Syst. Nanostruct. 41 (9) (2009) 1651–1655.
[15] L. Shen, H.-S. Shen, C.-L. Zhang, Nonlocal plate model for nonlinear vibration of single layer graphene sheets in thermal environments, Comput. Mater. Sci. 48 (3) (2010) 680–685.

[16] B. Arash, Q. Wang, A review on the application of nonlocal elastic models in modeling of carbon nanotubes and graphenes, Comput. Mater. Sci. 51 (1) (2012) 303–313.
[17] F.M. de Sciarra, M. Canadija, R. Barretta, A gradient model for torsion of nanobeams, C. R. Mecanique 343 (4) (2015) 289–300.
[18] D. Shahsavari, et al., Dynamic characteristics of viscoelastic nanoplates under moving load embedded within visco-Pasternak substrate and hygrothermal environment, Mater. Res. Express 4 (8) (2017) 085013.
[19] D. Shahsavari, M. Janghorban, Bending and shearing responses for dynamic analysis of single-layer graphene sheets under moving load, J. Braz. Soc. Mech. Sci. Eng. 39 (10) (2017) 3849–3861.
[20] B. Karami, M. Janghorban, L. Li, On guided wave propagation in fully clamped porous functionally graded nanoplates, Acta Astronaut. 143 (2018) 380–390.
[21] H. Zhang, C. Wang, N. Challamel, Modelling vibrating nano-strings by lattice, finite difference and Eringen's nonlocal models, J. Sound Vib. 425 (2018) 41–52.
[22] G.-L. She, et al., On vibrations of porous nanotubes, Int. J. Eng. Sci. 125 (2018) 23–35.
[23] G.-L. She, F.-G. Yuan, Y.-R. Ren, On wave propagation of porous nanotubes, Int. J. Eng. Sci. 130 (2018) 62–74.
[24] L. Li, Y. Hu, Torsional vibration of bi-directional functionally graded nanotubes based on nonlocal elasticity theory, Compos. Struct. 172 (2017) 242–250.
[25] X. Zhu, L. Li, Twisting statics of functionally graded nanotubes using Eringen's nonlocal integral model, Compos. Struct. 178 (2017) 87–96.
[26] B. Karami, et al., Thermal buckling of embedded sandwich piezoelectric nanoplates with functionally graded core by a nonlocal second-order shear deformation theory, Proc. Inst. Mech. Eng., Part C, J. Mech. Eng. Sci. (2018) 0954406218756451.
[27] D. Shahsavari, et al., On the shear buckling of porous nanoplates using a new size-dependent quasi-3D shear deformation theory, Acta Mech. (2018), article in press.
[28] M. Lazar, G.A. Maugin, E.C. Aifantis, On a theory of nonlocal elasticity of bi-Helmholtz type and some applications, Int. J. Solids Struct. 43 (6) (2006) 1404–1421.
[29] C.C. Koutsoumaris, et al., Application of bi-Helmholtz nonlocal elasticity and molecular simulations to the dynamical response of carbon nanotubes, in: AIP Conference Proceedings, AIP Publishing, 2015.
[30] M. Shaat, A. Abdelkefi, New insights on the applicability of Eringen's nonlocal theory, Int. J. Mech. Sci. 121 (2017) 67–75.
[31] R. Barretta, et al., Functionally graded Timoshenko nanobeams: a novel nonlocal gradient formulation, Composites, Part B, Eng. 100 (2016) 208–219.
[32] C. Lim, G. Zhang, J. Reddy, A higher-order nonlocal elasticity and strain gradient theory and its applications in wave propagation, J. Mech. Phys. Solids 78 (2015) 298–313.
[33] Q.-Y. Lin, et al., Stretch-induced stiffness enhancement of graphene grown by chemical vapor deposition, ACS Nano 7 (2) (2013) 1171–1177.
[34] X. Zhu, L. Li, On longitudinal dynamics of nanorods, Int. J. Eng. Sci. 120 (2017) 129–145.
[35] B. Karami, D. Shahsavari, L. Li, Hygrothermal wave propagation in viscoelastic graphene under in-plane magnetic field based on nonlocal strain gradient theory, Physica E, Low-Dimens. Syst. Nanostruct. 97 (2018) 317–327.
[36] E.C. Aifantis, Update on a class of gradient theories, Mech. Mater. 35 (3–6) (2003) 259–280.
[37] N. Challamel, C. Wang, The small length scale effect for a non-local cantilever beam: a paradox solved, Nanotechnology 19 (34) (2008) 345703.
[38] Y. Zhang, C. Wang, N. Challamel, Bending, buckling, and vibration of micro/nanobeams by hybrid nonlocal beam model, J. Eng. Mech. 136 (5) (2009) 562–574.
[39] A. Jafari, S.S. Shah-enayati, A.A. Atai, Size dependency in vibration analysis of nano plates; one problem, different answers, Eur. J. Mech. A, Solids 59 (2016) 124–139.
[40] F. Ebrahimi, M.R. Barati, A. Dabbagh, A nonlocal strain gradient theory for wave propagation analysis in temperature-dependent inhomogeneous nanoplates, Int. J. Eng. Sci. 107 (2016) 169–182.
[41] B. Karami, M. Janghorban, A. Tounsi, Nonlocal strain gradient 3D elasticity theory for anisotropic spherical nanoparticles, Steel Compos. Struct. 27 (2) (2018) 201–216.
[42] L. Li, Y. Hu, X. Li, Longitudinal vibration of size-dependent rods via nonlocal strain gradient theory, Int. J. Mech. Sci. 115–116 (2016) 135–144.
[43] B. Karami, M. Janghorban, A. Tounsi, Variational approach for wave dispersion in anisotropic doubly-curved nanoshells based on a new nonlocal strain gradient higher order shell theory, Thin-Walled Struct. 129 (2018) 251–264.
[44] H.B. Khaniki, S. Hosseini-Hashemi, Buckling analysis of tapered nanobeams using nonlocal strain gradient theory and a generalized differential quadrature method, Mater. Res. Express 4 (6) (2017) 065003.
[45] L. Li, H. Tang, Y. Hu, The effect of thickness on the mechanics of nanobeams, Int. J. Eng. Sci. 123 (2018) 81–91.
[46] M.R. Nami, M. Janghorban, Resonance behavior of FG rectangular micro/nano plate based on nonlocal elasticity theory and strain gradient theory with one gradient constant, Compos. Struct. 111 (2014) 349–353.
[47] B. Karami, et al., Wave dispersion of mounted graphene with initial stress, Thin-Walled Struct. 122 (2018) 102–111.
[48] D. Shahsavari, B. Karami, S. Mansouri, Shear buckling of single layer graphene sheets in hygrothermal environment resting on elastic foundation based on different nonlocal strain gradient theories, Eur. J. Mech. A, Solids 67 (2018) 200–214.
[49] B. Karami, et al., Hygrothermal wave characteristic of nanobeam-type inhomogeneous materials with porosity under magnetic field, Proc. Inst. Mech. Eng., Part C, J. Mech. Eng. Sci. (2018) 0954406218781680.
[50] B. Karami, M. Janghorban, A. Tounsi, Effects of triaxial magnetic field on the anisotropic nanoplates, Steel Compos. Struct. 25 (3) (2017) 361–374.
[51] B. Karami, D. Shahsavari, L. Li, Temperature-dependent flexural wave propagation in nanoplate-type porous heterogenous material subjected to in-plane magnetic field, J. Therm. Stresses 41 (4) (2018) 483–499.
[52] M.R. Barati, On wave propagation in nanoporous materials, Int. J. Eng. Sci. 116 (2017) 1–11.
[53] M.R. Barati, A. Zenkour, A general bi-Helmholtz nonlocal strain-gradient elasticity for wave propagation in nanoporous graded double-nanobeam systems on elastic substrate, Compos. Struct. 168 (2017) 885–892.
[54] A. Farajpour, et al., A higher-order nonlocal strain gradient plate model for buckling of orthotropic nanoplates in thermal environment, Acta Mech. 227 (7) (2016) 1849–1867.
[55] B. Karami, et al., A size-dependent quasi-3D model for wave dispersion analysis of FG nanoplates, Steel Compos. Struct. 28 (1) (2018) 99–110.
[56] H.-S. Shen, L. Shen, C.-L. Zhang, Nonlocal plate model for nonlinear bending of single-layer graphene sheets subjected to transverse loads in thermal environments, Appl. Phys. A, Mater. Sci. Process. 103 (1) (2011) 103–112.
[57] D.D. Han, et al., Moisture-responsive graphene paper prepared by self-controlled photoreduction, Adv. Mater. 27 (2) (2015) 332–338.
[58] E.O. Alzahrani, A.M. Zenkour, M. Sobhy, Small scale effect on hygro-thermo-mechanical bending of nanoplates embedded in an elastic medium, Compos. Struct. 105 (2013) 163–172.
[59] F. Ebrahimi, M.R. Barati, Hygrothermal effects on vibration characteristics of viscoelastic FG nanobeams based on nonlocal strain gradient theory, Compos. Struct. 159 (2017) 433–444.
[60] D. Shahsavari, et al., A novel quasi-3D hyperbolic theory for free vibration of FG plates with porosities resting on Winkler/Pasternak/Kerr foundation, Aerosp. Sci. Technol. 72 (2018) 134–149.
[61] R. Kolahchi, M. Safari, M. Esmailpour, Dynamic stability analysis of temperature-dependent functionally graded CNT-reinforced visco-plates resting on orthotropic elastomeric medium, Compos. Struct. 150 (2016) 255–265.

[62] S. Pouresmaeeli, E. Ghavanloo, S. Fazelzadeh, Vibration analysis of viscoelastic orthotropic nanoplates resting on viscoelastic medium, Compos. Struct. 96 (2013) 405–410.
[63] H.F. Brinson, L.C. Brinson, Polymer Engineering Science and Viscoelasticity, Springer, 2008.
[64] A.G. Arani, et al., Nonlocal vibration of coupled DLGS systems embedded on visco-Pasternak foundation, Physica B, Condens. Matter 407 (21) (2012) 4123–4131.
[65] B. Karami, M. Janghorban, Effect of magnetic field on the wave propagation in nanoplates based on strain gradient theory with one parameter and two-variable refined plate theory, Mod. Phys. Lett. B 30 (36) (2016) 1650421.
[66] P. Malekzadeh, A. Setoodeh, A.A. Beni, Small scale effect on the thermal buckling of orthotropic arbitrary straight-sided quadrilateral nanoplates embedded in an elastic medium, Compos. Struct. 93 (8) (2011) 2083–2089.
[67] J.E. Lagnese, Boundary Stabilization of Thin Plates, SIAM, 1989.
[68] A.D. Drozdov, Viscoelastic Structures: Mechanics of Growth and Aging, Academic Press, 1998.
[69] L. Li, et al., Dynamics of structural systems with various frequency-dependent damping models, Front. Mech. Eng. 10 (1) (2015) 48–63.
[70] L. Li, Y. Hu, Wave propagation in fluid-conveying viscoelastic carbon nanotubes based on nonlocal strain gradient theory, Comput. Mater. Sci. 112 (2016) 282–288.
[71] M. Sobhy, Hygrothermal deformation of orthotropic nanoplates based on the state-space concept, Composites, Part B, Eng. 79 (2015) 224–235.
[72] M. Sobhy, Hygrothermal vibration of orthotropic double-layered graphene sheets embedded in an elastic medium using the two-variable plate theory, Appl. Math. Model. 40 (1) (2016) 85–99.
[73] H. Ma, X.-L. Gao, J. Reddy, A microstructure-dependent Timoshenko beam model based on a modified couple stress theory, J. Mech. Phys. Solids 56 (12) (2008) 3379–3391.
[74] W. Xiao, L. Li, M. Wang, Propagation of in-plane wave in viscoelastic monolayer graphene via nonlocal strain gradient theory, Appl. Phys. A 123 (6) (2017) 388.
[75] M. Mohr, et al., Phonon dispersion of graphite by inelastic X-ray scattering, Phys. Rev. B 76 (3) (2007) 035439.